PAPER

Influence of synthesis conditions on the surface passivation and electrochemical behavior of layered cathode materials†

Feng Lin,*[a] Dennis Nordlund,[b] Taijun Pan,[ac] Isaac M. Markus,[ad] Tsu-Chien Weng,[b] Huolin L. Xin*[e] and Marca M. Doeff*[a]

Understanding the relationship between materials synthesis and electrochemical behaviors should provide valuable knowledge to further the advancement of lithium-ion batteries. In this work, layered cathode materials {*e.g.*, $LiNi_{0.4}Mn_{0.4}Co_{0.18}Ti_{0.02}O_2$ (NMCs)} were prepared under three different annealing conditions, *i.e.*, 900 °C for 6 hours, 8 hours, and 12 hours, respectively. The resulting materials exhibit equivalent crystal structures and morphologies yet likely different surface chemical environments. These materials show distinctively different resistances against the surface passivation/reconstruction (reduction of the transition metals in the layered structure to form rock-salt and/or spinel phases) during electrochemical cycling (2.0–4.7 V *vs.* Li^+/Li). In general, the materials annealed for longer durations exhibited lower tendencies to form the surface passivation layer. Furthermore, the surface passivation became less severe when the electrode materials were cycled under mild conditions, such as slow constant current charging–discharging as opposed to cyclic voltammetry. The present study correlates the synthetic conditions with the surface instability and the electrochemical performance in cathode materials, and provides new insights into improving synthetic protocols for battery materials.

Introduction

Advances in lithium-ion battery technologies for emerging vehicular applications are largely driven by improved knowledge of the design and synthesis of battery materials. There have been several major breakthroughs in materials design since the commercialization of lithium-ion batteries.[1–3] To date, however, cathode materials are still considered the major limitation to the achievement of high energy density lithium-ion batteries.[4] The preparation of cathode materials requires precise controls for lithium stoichiometry,[5] cation mixing,[6] and surface chemical environments.[7,8] High-temperature annealing is essential for synthesizing crystalline cathode materials with well-defined lithium diffusion

channels.[5,9] The annealing temperature, ramping rate, and duration potentially play significant roles in determining the electrochemical properties of the resulting materials. A successful synthesis should yield high energy density cathode materials with minimal electrode–electrolyte side reactions in conventional liquid electrolytes. Stoichiometric layered materials {*e.g.*, $LiNi_{1-x-y}Mn_xCo_yO_2$ (NMCs)} represent a class of cathode materials with potential for use at high voltages to increase practical energy densities. The reliability of NMC materials at high voltages is strongly governed by the structural and chemical stability at the particle surfaces.[10–12] The particle surfaces usually undergo undesirable structural and chemical evolution (surface passivation) under harsh cycling conditions, such as high-voltage cycling. One of the major passivation mechanisms is surface reconstruction through the reduction of transition metals to form rock-salt and/or spinel phases. The passivation layer forms during the first charge,[12] and during exposure to electrolytic solution,[10,12] and accumulates during extended charging–discharging cycles.[10,11] The passivation layer inhibits lithium diffusion kinetics and increases the overall cell impedance, leading to the loss of practical capacity at moderate discharge rates. However, it has been shown that the lost capacity can mostly be recovered when a much slower charging rate is adopted.[10] The surface chemical environment inherited from the synthesis can potentially influence the generation of the

[a] *Environmental Energy Technologies Division, Lawrence Berkeley National Laboratory, Berkeley, CA 94720, USA. E-mail: flin@lbl.gov; mmdoeff@lbl.gov*

[b] *Stanford Synchrotron Radiation Lightsource, SLAC National Accelerator Laboratory, Menlo Park, CA 94025, USA*

[c] *School of Materials Science and Engineering, Changzhou University, Changzhou 213164, China*

[d] *Department of Materials Science and Engineering, University of California, Berkeley 94720, USA*

[e] *Center for Functional Nanomaterials, Brookhaven National Laboratory, Upton, NY 11973, USA. E-mail: hxin@bnl.gov*

† Electronic supplementary information (ESI) available. See DOI: 10.1039/c4ta04497e

This journal is © The Royal Society of Chemistry 2014

J. Mater. Chem. A, 2014, **2**, 19833–19840 | **19833**

surface passivation later in the electrochemical processes.[13,14] To date, however, the correlation between synthetic conditions and the electrochemistry-induced surface passivation has not been demonstrated in the literature. Such a study may provide valuable knowledge to guide the general design and synthesis of battery materials.

The present study was designed to study the correlation between the synthetic conditions and the surface stability of NMC materials undergoing electrochemical cycling. The degree of the surface passivation is directly associated with the duration of thermal annealing and is influenced by the conditions of electrochemical cycling. As described herein, we found that longer annealing duration and constant current cycling are beneficial for the preservation of the surface structural integrity.

Experimental

Synthesis

The composition $LiNi_{0.4}Mn_{0.4}Co_{0.18}Ti_{0.02}O_2$ (NMC442–2%Ti) was targeted for this study. Materials were synthesized using a co-precipitation method described in our previous study.[10] For the synthesis, 250 mL of an aqueous solution of transition metal nitrates 0.16 M $Ni(NO_3)_2$, 0.16 M $Mn(NO_3)_2$, 0.072 M $Co(NO_3)_2$, 0.008 M $TiO(SO_4) \cdot xH_2O$ and 250 mL of 0.8 M LiOH aqueous solution were dripped simultaneously into a beaker using a Masterflex C/L peristaltic pump and stirred continuously. The chemicals were purchased from Sigma Aldrich without any further purification. The precipitate was collected, filtered and washed with DI water, and then dried overnight at 100 °C in the oven. The dried precipitate was ball-milled (1 atm, 500 rpm, 1 hour) with LiOH, where 5% extra LiOH was added to account for the lithium loss in the subsequent annealing. The ball-milled mixture was then separated into three batches and each of them was heated in air up to 900 °C ramping from room temperature to 900 °C in 8 hours, maintained at the temperature for 6 hours, 8 hours and 12 hours, respectively, and finally cooled down to room temperature naturally. The annealing was performed in Coors high-alumina crucibles in a Thermo Scientific BF51848A-1 Lindberg/Blue M moldatherm box furnace with an integrated single-program/multi-segment programmable digital controller with over-temperature protection. Other parameters, such as ramping, batch size and crucible size, were strictly controlled to be identical.

Electrode preparation and electrochemical measurement

Composite electrodes were prepared with 84 wt% active material, 8 wt% polyvinylidene fluoride (Kureha Chemical Ind. Co. Ltd), 4 wt% acetylene carbon black (Denka, 50% compressed) and 4 wt% SFG-6 synthetic graphite (Timcal Ltd, Graphites and Technologies) in N-methyl-2-pyrrolidinone and cast onto carbon-coated aluminum current collectors (Exopack Advanced Coatings (http://www.exopackadvancedcoatings.com)) with typical active material loadings of 4–6 mg cm^{-2} 2032-type coin cells were assembled in a helium-filled glove box using the composite electrode as the positive electrode and Li metal as the negative electrode. A Celgard 2400 separator and 1 M $LiPF_6$

electrolyte solution in 1 : 2 w/w ethylene carbonate/dimethyl carbonate (Ferro Corporation) were used to fabricate the coin cells. Battery testing was performed on a computer controlled VMP3 potentiostat/galvanostat (BioLogic). Cyclic voltammetry was performed between 2.0 V and 4.7 V vs. Li$^+$/Li using a scan rate of 0.5 mV s^{-1}. Galvanostatic cycling was performed at C/13 between 2.0 V and 4.7 V vs. Li$^+$/Li. 1C was defined as fully charging a cathode in 1 h, corresponding to a specific current density of 280 mA g^{-1}. The voltage range (2.0–4.7 V vs. Li$^+$/Li) was used according to our previous studies.[10,15,16] The electrodes were removed from coin cells, rinsed with dimethyl carbonate and dried in a helium-filled glove box for further study. The electrodes were sealed under helium and then transferred to the synchrotron beamline using a homemade system to prevent air/moisture exposure. For electron microscopy and spectroscopy measurements, the electrode particles were scratched off and deposited onto TEM grids.

Materials characterization

X-ray Diffraction (XRD) on powder samples was performed on a Phillips X'Pert diffractometer with an X'celerator detector using Cu K$_\alpha$ radiation. The powder diffraction patterns were typically scanned over an angular range of 10–80° (2θ) with a step size of 0.01°. Scanning electron microscopy (SEM) was performed on a JEOL JSM-7000F with a Thermo Scientific Inc. EDS (energy dispersive X-ray spectroscopy) detector. BET measurements were carried out on a Tristar 3000 surface area & porosity analyzer (Micromeritics Instrument Corp). X-ray absorption spectroscopy (XAS) measurements were performed on the 31-pole wiggler beamline 10-1 at Stanford Synchrotron Radiation Lightsource (SSRL) using a ring current of 350 mA and a 1000 l mm^{-1} spherical grating monochromator with 20 μm entrance and exit slits, providing ~10^{11} ph s^{-1} at 0.2 eV resolution in a 1 mm^2 beam spot. During the measurements, all battery electrode samples were attached to an aluminum sample holder using conductive carbon tape (X-ray beam probing the top surface of the composite electrodes). For the pristine samples, the XAS measurements were performed on powder samples deposited on the conductive carbon tape. Data were acquired under ultrahigh vacuum (10^{-9} Torr) in a single load at room temperature using total electron yield (TEY), Auger electron yield (AEY) and fluorescence yield (FY). The sample drain current was collected for TEY. Auger electron yield (AEY) was collected with a Cylindrical Mirror Analyzer using a pass energy of 200 eV and a kinetic energy window of 2 eV near the main Auger for oxygen and nitrogen, respectively. A silicon diode (IRD AXUV-100) was used to collect the fluorescence yield (FY) positioned near the sample surface. Contributions from visible light were carefully minimized before the acquisition, and all spectra were normalized by the current from freshly evaporated gold on a fine grid positioned upstream of the main chamber. Two probe-corrected field-emission scanning transmission electron microscopes (STEM) operated at 200 keV and 300 keV were used for annular dark-field STEM (ADF-STEM) imaging and spatially resolved electron energy loss spectroscopy (EELS).

Results and discussion

Powder X-ray diffraction (XRD) confirmed that the NMC materials have the expected $R\bar{3}m$ layered structure (Fig. 1), and these materials show very minor differences in the crystallinity, as shown by their equivalent reflection peak widths. For samples without preferred crystal orientation and the same compositions, the ratio between the integrated intensities of (003) and (104) peaks is an approximate measure of the amount of cation mixing.[6] Here, the ratio has a nearly constant value of 1.0 for all the samples, indicating that the degree of transition metal–lithium ion intermixing remained roughly constant within these samples. The lattice parameters were estimated by Rietveld refinement (Fig. S1†), and the results are tabulated in Table S1.† The refinement results show there was indeed no major difference in the ion intermixing, and the sample annealed for 6 hours showed the smallest lattice parameters.

The morphologies and chemical compositions of the resulting materials were studied by SEM-EDS. The transition metal ratios stayed constant in these materials, because they were prepared from the same batch of mixed hydroxide precursor. EDS elemental mapping provided an estimate of the chemical composition for the materials: Ni ∼ 43.0%, Co ∼ 16.9%, Mn ∼ 37.8% and Ti ∼2.3%, close to the targeted composition, and to that reported by Kam et al. using a similar synthetic protocol.[16] The deviation from the targeted composition is likely due to the different precipitation rates of transition metal ions. There is no appreciable difference among these samples in terms of particle morphology and size; in general, the particles exhibited irregular shapes and ranged from 100–400 nm in size. Given the fact that these materials are not porous, the surface area is a good estimate for the average particle size; the N_2 physisorption Brunauer–Emmett–Teller (BET) analysis confirmed that these materials had a similar surface area of approximately 3.0 m^2 g^{-1} (N_2 physisorption curves are provided in Fig. S2† and suggest no defined pore structures in these materials). Therefore, changes in the annealing time had little effect on the particle morphology (Fig. 2a–c and BET) or bulk crystal structure (Fig. 1).
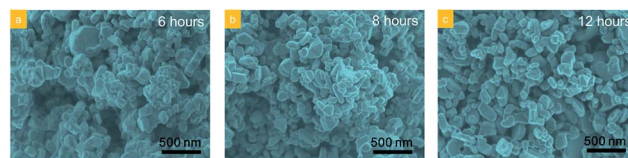
Fig. 2 SEM results of the NMC442–2%Ti samples undergoing thermal annealing for different periods of time: (a) 6 hours at 900 °C, (b) 8 hours at 900 °C, and (c) 12 hours at 900 °C.

A prolonged annealing duration could possibly influence the chemical environment at the surfaces of battery materials, which then substantially alters the structural evolution of electrode materials in the electrochemical cycling and leads to different cycling performances. Fig. 3 shows the surface sensitive soft XAS spectra (TEY mode, which probes the top 2–5 nm) for the materials annealed for different lengths of time in the pristine state. The transition metal XAS spectra are independent of the annealing duration; nickel, cobalt, and manganese show oxidation states of Ni^{2+}, Co^{3+} and Mn^{4+} in all these materials (Fig. 3a–c). The O K-edge XAS spectra, however, show slight differences in these materials. These can be divided into two regions, as shown in Fig. 3d corresponding to hybridized states between TM3d–O2p and TM4sp–O2p in the TMO_6 octahedral unit, respectively. A complete deconvolution of the spectra to Ni–O, Co–O and Mn–O hybridized states was not attempted due to the complex arrangement of the transition metals in the NMC lattice. However, salient information could be extracted from the TM3d–O2p pre-edge feature, which is determined by the t_{2g}–e_g occupancy and TM–O covalency.[17,18] The O K-edge XAS spectra reveal that there are different oxygen electronic structures (t_{2g}–e_g occupancy and TM–O covalency) on the surfaces of these materials. This is possibly explained by the presence of slight lithium excess on the surfaces of particles in the material annealed for a short length of time (6 hours), because the TM3d–O2p hybridization is interrupted by the presence of lithium in the TM 3b sites. The XAS measurement with a 50 nm depth sensitivity (FY mode) provided similar electronic information to the TEY mode.

Cyclic voltammetry (CV) is a sensitive diagnostic tool for studying redox couples, observing changes in cycling behavior, and detecting impurity phases. Fig. 4 show the CV curves for the cells containing NMC442–2%Ti materials annealed for 6 hours, 8 hours, and 12 hours at 900 °C in air. There are distinctly different behaviors observed for these electrodes in terms of curve shape, peak position and cycling stability. In the first cycle, there is an obvious extra oxidation peak at 4.5 V vs. Li^+/Li (marked by #) in the CV curve in the sample annealed for only 6 hours, not observed in the sample annealed for 8 hours or 12 hours. A high voltage formation process associated with Li and O loss (or oxidation) is normally observed during the first cycle of cells containing Li-excess and Li and Mn excess NMCs (LMR–NMCs),[19–22] similar to what is observed here. However, non-stoichiometric compositions were not targeted for these samples, which, were, in any case, were made from the same batch of precursor material, and differed only in annealing
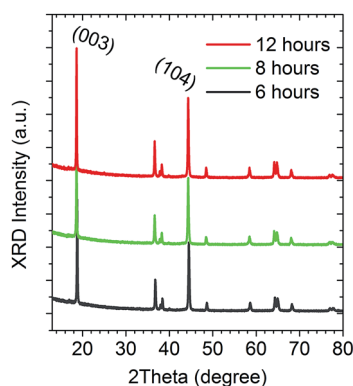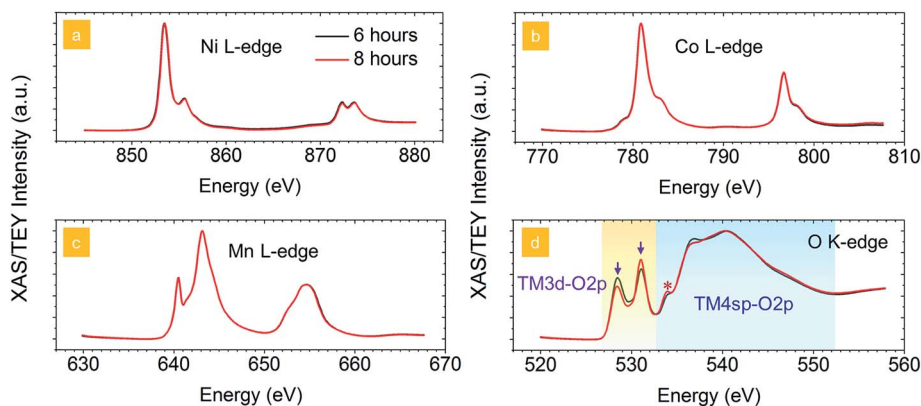

Fig. 1 XRD patterns of NMC442–2%Ti materials prepared with different annealing durations at 900 °C: 6 hours (black), 8 hours (green) and 12 hours (red).

Fig. 3 Soft XAS spectra of (a) Ni L-edge, (b) Co L-edge, (c) Mn L-edge and (d) O K-edge for the pristine NMC442−2%Ti materials, where the gray and red curves represent the samples with 6 hours and 8 hours of annealing, respectively. The (*) marks the characteristic feature for the oxygen from the conductive carbon tapes. The measurements were performed using the TEY mode.
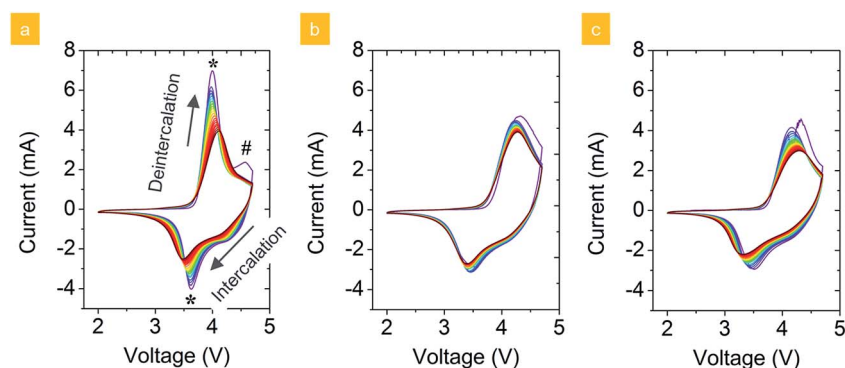

Fig. 4 Cyclic voltammetry of cells containing the NMC442−2%Ti samples annealed for different lengths of time between 2.0 V and 4.7 V $vs.$ Li$^+$/Li: (a) 6 hours at 900 °C, (b) 8 hours at 900 °C, and (c) 12 hours at 900 °C. The (*) marks indicate cathodic and anodic peaks and the (#) mark may be associated with Li and O loss (or oxidation) due to slight lithium excess on particle surfaces in this material. The scanning was started with delithiation from the open circuit voltage and the arrows in (a) indicate the scanning direction. The highest peak deintercalation current density in (a) was approximately 3.6 mA cm^{-2} (860 mA g^{-1}).

time. The O K-edge data shown in Fig. 3d implies that a slight lithium-excess may be present on the surfaces of particles annealed for 6 hours, which may explain this feature. Initially, the sample annealed for 6 hours showed sharper redox peaks and a smaller voltage separation between the cathodic and anodic peaks than the ones annealed for 8 hours and 12 hours. Upon cycling, however, the peaks decreased in intensity and broadened more rapidly than those in the CVs of the cells containing the samples annealed for 8 or 12 hours. The oxidation peaks also gradually shifted to higher potentials, whereas the reduction peaks shifted to lower ones, indicating that the polarization in this cell increased upon cycling to a greater degree than in the other cells. The CV results suggest that the electrode containing the sample annealed for 6 hours underwent degradation that hindered the lithium diffusion kinetics and/or led to the loss of electrochemically active phase in this voltage range (2.0–4.7 V $vs.$ Li$^+$/Li).

Discharge capacities and coulombic efficiencies were calculated from the cyclic voltammetry cycling, and the results are shown in Fig. 5a and b, respectively. The first-cycle discharge

capacities for the cells were 200 mA h g^{-1} (sample annealed for 6 hours), 190 mA h g^{-1} (sample annealed for 8 hours), and 176 mA h g^{-1} (sample annealed for 12 hours). All the samples exhibited gradual capacity fading, but that of the sample annealed for 8 hours showed the slowest fading rate. The capacity fading was more severe than the electrodes cycled to lower voltages, such as 4.3 V $vs.$ Li$^+$/Li.[1,10] The first cycle coulombic inefficiencies ranged from approximately 9–12% for all of the cells but those containing samples annealed for longer durations exhibited higher first cycle coulombic efficiencies. This apparent irreversibility is commonly observed in electrochemical cells containing NMCs regardless of the upper voltage limit used,[23] although it is generally higher when cells are charged to high voltages (e.g., 4.7 V $vs.$ Li$^+$/Li).[15] Although the coulombic efficiency was slightly improved as the cycling continued (Fig. 5b), it is still not satisfactory compared to the electrodes cycled to lower voltages. It has been partially ascribed to a surface structural reconstruction that occurs either during the initial cell charge or upon prolonged exposure to electrolytic solution.[10,12] The coulombic efficiencies improved after the

19836 | J. Mater. Chem. A, 2014, **2**, 19833–19840

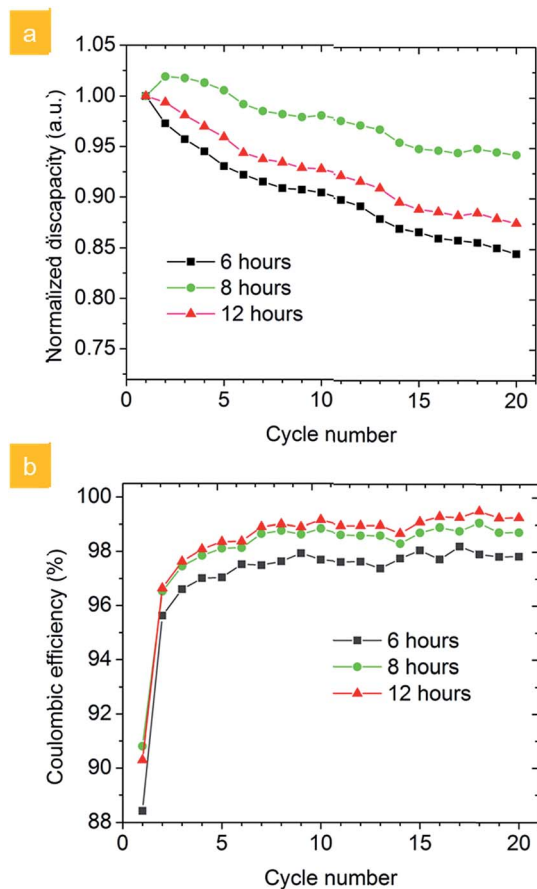This journal is © The Royal Society of Chemistry 2014

Fig. 5 The calculated (a) normalized discharge capacities and (b) coulombic efficiencies for the samples annealed for different periods of time and cycled in electrochemical cells for 20 CV cycles between 2.0–4.7 V vs. Li$^+$/Li. The initial discharge capacities for the samples are 200 mA h g^{-1} (6 hours), 190 mA h g^{-1} (8 hours), and 176 mA h g^{-1} (12 hours).
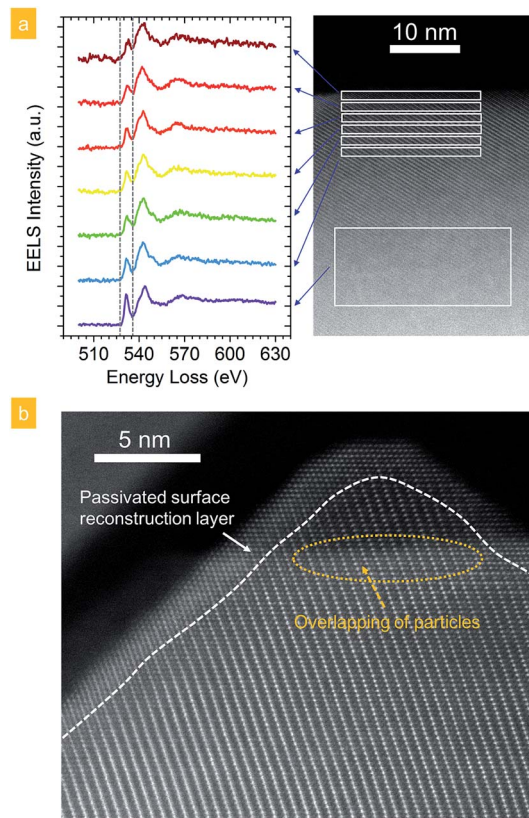

Fig. 6 (a) STEM-EELS spectra of the regions enclosed in boxes in an NMC442–2%Ti (annealed 6 hours) particle after one electrochemical cycle (in the discharged state). The pre-edge feature between the two dashed lines is attributable to the electronic transition from the O1s orbital to that of the O2p that is hybridized with TM3d. (b) ADF-STEM image of an NMC particle nearly on the $R\bar{3}m$ [100] zone axis; the dashed line provides an approximate boundary between the surface passivation layer (mixed spinel/rock-salt phase) and the bulk layered NMC structure. Note that there is a particle-overlapping region in the ADF-STEM image, outlined by the orange dashed ellipse.

second cycles for all the cells, as is typical for those containing NMCs, and the cells containing samples annealed for longer durations (8 hours and 12 hours) provided higher coulombic efficiencies in each cycle.

The capacity fading for the cells shown in Fig. 5 is similar to previous results reported in the literature, and is also typical of NMCs cycled to high potentials. The structural changes in NMC particle surfaces continue upon cycling, and propagate more severely when voltage limits are high.[10,11] Although very little material is transformed during early cycles, the structural changes result in increased cell impedance, which reduces the practical capacity. After twenty cycles, it has been shown that most of the capacity can be regained by discharging at low current densities, indicating that the amount of material transformed is actually very small.[10]

To better understand the effects of annealing time, the materials were studied by scanning transmission electron microscopy coupled with electron energy loss spectroscopy (STEM-EELS) after one electrochemical cycle, and representative results are shown in Fig. 6. The hybridization of TM3d–O2p orbitals allowed us to probe unoccupied 3d states in transition

metals by examining the O K-edge EELS,[24–27] although the energy resolution of EELS does not allow for more subtle analysis. We observed that the average TM oxidation state decreased upon moving from the bulk towards the edge of the particle, as evidenced by the decrease of oxygen TM3d–O2p pre-edge intensity (between the two dashed lines, Fig. 6a). This phenomenon is attributable to a transition from a layered structure to a mixed rock-salt/spinel structure at surfaces of the studied particles (Fig. 6b), which implies the loss of lithium and oxygen, similar to what occurs in LMR–NMCs.[28] This phase transition may be driven by the intrinsic instability of the layered structure at high voltages (extended lithium removal from the NMC lattice[12,29]) as well as interactions between the electrode and the electrolytic solution.[10]

Due to the limited number of particles that can be studied using STEM-EELS, it is a formidable challenge to obtain ensemble-averaged information at the electrode level. In contrast, synchrotron X-ray experiments can be tuned with a beam size of mm^2 and are capable of probing multiple spots in a single load, thereby providing complementary electronic

information at a macroscopic length scale. Both hard and soft XAS has been widely adopted to track the change of electronic structures in battery materials.[30,31] An advantage of soft XAS is the ability to investigate electronic structures of elements from surfaces to bulk, depending on the experimental setup. Probing depths range from about 1–2 nm for Auger electron yield (AEY) and 2–5 nm for total electron yield (TEY), to about 50 nm (or bulk) for fluorescence electron yield (FY). A gradient in the TM oxidation states (*i.e.*, occupancies of 3d orbitals) from surfaces into the bulk has been observed in cycled NMC electrodes and correlates with capacity fading in electrochemical cells.[10,12] In pristine NMC442–2%Ti materials, the oxidation states of nickel, manganese, and cobalt are 2+, 4+ and 3+, respectively, and upon charging, nickel and, sometimes, cobalt are oxidized depending on composition and potential limits. In rock-salt structures (TMO) the transition metals are primarily in 2+ oxidation states. Thus the electronic structure changes observed in the XAS spectra can be used to verify the surface reconstruction observed in specific particles in the STEM imaging (Fig. 6b) for the bulk samples on average. Fig. 7 shows the soft XAS results, comparing the evolution of the electronic structures upon electrochemical cycling. Nickel is the primary active component in the NMC442–2%Ti materials under our experimental conditions. During the charging (lithium deintercalation) and discharging (lithium intercalation) processes, nickel switches between Ni^{2+} and $Ni^{(2+x)+}$ oxidation states, where the *x* value is usually determined by the degree of lithium deintercalation, *i.e.*, charging voltage cutoff in the galvanostatic or potentiostatic cycling.[12,24,31,32] At the end of discharge, the nickel oxidation state returns to Ni^{2+} independent of changes in the crystal structure (Fig. 7a), so that detection of Ni^{2+} in the TEY data is not proof *per se* of surface reconstruction to the rock salt structure. However, obvious changes were observed in the Mn L-edge and Co L-edge XAS TEY spectra after the electrodes were cycled. The oxidation states of these TMs can be determined by examining the fine structures of L3,2 absorption edges. The lower-energy shoulder of the Co L3-edge intensified when the materials were cycled, with the most significant increase observed in the material that was annealed for only 6 hours (Fig. 7b). The increased lower-energy feature in the Co L3-edge represents a decrease in the cobalt oxidation state.[10] The depth-profiled XAS study demonstrated that the decrease of oxidation state is more pronounced towards particle surfaces, as shown in Fig. 7c. Manganese underwent a similar surface reduction upon cycling (Fig. 7d), as revealed by the low-energy shoulder of the Mn L3-edge, as well as by the L3/L2 intensity ratio, another benchmark useful for analyzing the oxidation states of TMs.[33] In 3d TMs with d occupancies lower than $3d^5$, the L3/L2 intensity ratio is generally in a positive relationship with the *d* occupancy; *i.e.*, inversely related to the oxidation state.[33] In this study, we observed an increased L3/L2 intensity ratio for Mn after extended CV cycles, indicating that manganese had been reduced (Fig. 7e). Furthermore, manganese reduction primarily occurred at the surface (Fig. 7f). Therefore, the electrochemically induced oxidation state gradients in TMs and the structural transition primarily occurred at particle surfaces, as schematically shown in Fig. 7g. The fraction of the surface structural transition is too small to be detected by bulk sensitive
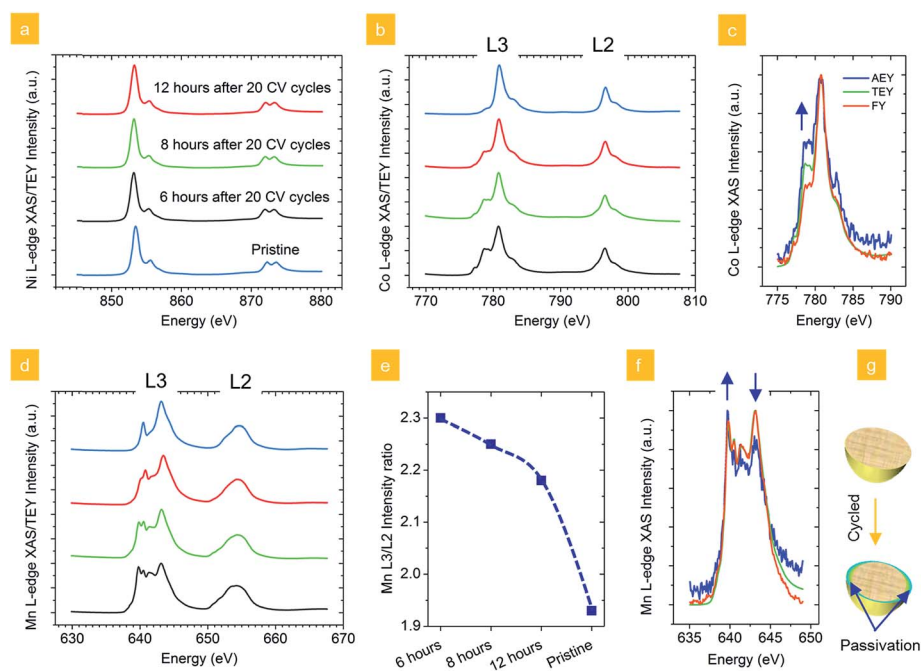

Fig. 7 Soft XAS results of the samples after being cycled 20 times using cyclic voltammetry and stopped at the end of discharge: (a) Ni L-edge in the TEY mode, (b) Co L-edge in the TEY mode, (c) Co L3-edge of the sample annealed for 6 hours after 20 CV cycles in AEY, TEY and FY modes, (d) Mn L-edge in the TEY mode, (e) Mn L3/L2 ratios from the various spectra in (d), (f) Mn L3-edge of the sample annealed for 6 hours after 20 CV cycles and (g) schematic representation for the gradient distribution of transition metal oxidation states. Spectra collected from different samples are labeled using different colors in (a–c): pristine sample (cyan), samples annealed for 6 hours (black), 8 hours (green), 12 hours (red) after 20 CV cycle.

techniques, such as XRD and hard XAS. Under the annealing conditions used in this study, there is a lower tendency to form the surface reduced layer in the samples prepared with a longer annealing duration (12 hours). Furthermore, the increased build-up of the surface reduced layer seen for the samples annealed for 6 hours is associated with more severe capacity fading during the CV cycling, similar to what is observed when NMC materials were cycled galvanostatically using the same voltage limits.[10] There are also other parameters influencing the cycling behavior, such as electrolyte decomposition at high voltages (*e.g.*, 4.7 V *vs.* Li$^+$/Li),[10,12] which may explain the better capacity retention observed in the cell containing the sample annealed for 8 hours compared to that containing one annealed for 12 hours. The coulombic inefficiency in each cycle seems to be directly related to the thickness of the surface reduced layer as well; a shorter annealing duration for the NMC-2%Ti material resulted in a thicker surface reduced layer and thus a poorer coulombic efficiency (Fig. 5b and 7).

Previous studies showed that the surface passivation layer could be generated simply by exposing electrode materials to the electrolytic solution; *e.g.*, LiPF$_6$ dissolved in EC–DMC.[10,12] Here we show that the passivation build-up is also influenced by the electrochemistry technique used in the charging–discharging processes. Two identical electrodes were cycled using cyclic voltammetry and galvanostatic cycling (GCPL) between 2 V and 4.7 V *vs.* Li$^+$/Li for 20 cycles (20 CV cycles took ~60 hours, whereas 20 GCPL took ~300 hours). They showed substantial differences in the thicknesses of the surface passivation layers. Although the electrode cycled using cyclic voltammetry spent much less time submerged in the electrolytic solution, the electrode had a thicker surface passivation layer, as evidenced by the higher intensities at the lower energy shoulders of both Mn L3-edge and Co L3-edge spectra (Fig. 8). We speculate that temporarily high current densities induced by potential sweeping during the CV experiment resulted in more severe surface reconstruction, but further study is needed to verify this. Clearly, however, the method of lithium intercalation and deintercalation also influences the surface passivation of NMC materials as well as details of the synthesis.

Conclusion

In summary, we have shown how cathode materials with identical compositions and similar bulk structures and particle morphologies can behave dissimilarly during electrochemical cycling (2.0–4.7 V *vs.* Li$^+$/Li). NMC materials typically undergo surface reconstruction to rock salt and spinel structures containing reduced transition metals upon prolonged exposure to electrolytic solutions or electrochemical cycling, which is more severe when higher voltage limits are used. The surface reconstruction is correlated with coulombic inefficiencies and capacity fading during repeated cycling to high potentials. In general, longer annealing durations for the NMC442–2%Ti materials resulted in thinner surface passivation layers, higher coulombic efficiencies and better capacity retention during high voltage cycling in lithium cells. The development of the surface reconstruction layer on the NMC materials was also influenced by the electrochemical technique used to cycle cells with cyclic voltammetry resulting in thicker reconstruction layers than the galvanostatic cycling, even though the exposure time to the electrolyte was drastically shorter in the former. These results illustrate the complex effects and interplay of synthesis and electrochemical history upon performance of NMC materials.

Conflict of interest

The authors declare no competing financial interests. This document was prepared as an account of work sponsored by the United States Government. While this document is believed to contain correct information, neither the United States Government nor any agency thereof, nor the Regents of the University of California, nor any of their employees, makes any warranty, express or implied, or assumes any legal responsibility for the accuracy, completeness, or usefulness of any information, apparatus, product, or process disclosed, or represents that its use would not infringe privately owned rights. Reference herein to any specific commercial product, process, or service by its trade name, trademark, manufacturer, or otherwise, does not necessarily constitute or imply its endorsement, recommendation, or favoring by the United States Government or any agency
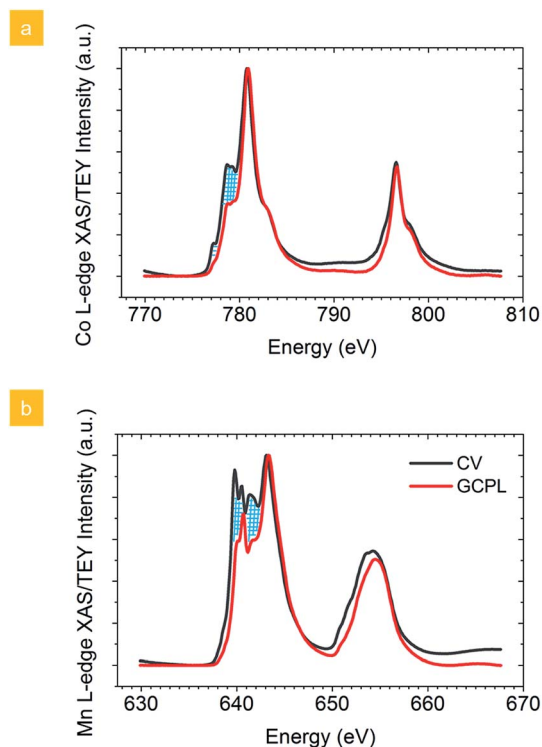
Fig. 8 Comparison of (a) Co L-edge and (b) Mn L-edge in NMC442–2%Ti (annealed for 6 hours) electrodes cycled for 20 cycles using CV (gray) or constant current conditions (red). The major spectral differences are marked with cross-hatching in (a) and (b). The measurements were performed using the TEY mode. The current density for the constant current cycling was approximately 0.11 mA cm^{-2} (21.4 mA g^{-1}). The first cycle discharge capacity and coulombic inefficiency were 192 mA h g^{-1} and 16.8%, respectively.

This journal is © The Royal Society of Chemistry 2014

J. Mater. Chem. A, 2014, **2**, 19833–19840 | **19839**

References

1 M. S. Whittingham, *Chem. Rev.*, 2004, **104**, 4271–4302.

2 M. M. Doeff, *Batteries: Overview of Battery Cathodes*, Springer, New York, 2013.

3 P. Poizot, S. Laruelle, S. Grugeon, L. Dupont and J. M. Tarascon, *Nature*, 2000, **407**, 496–499.

4 A. Manthiram, *J. Phys. Chem. Lett.*, 2011, **2**, 176–184.

5 G. Chen, B. Hai, A. K. Shukla and H. Duncan, *J. Electrochem. Soc.*, 2012, **159**, A1543–A1550.

6 S. Patoux and M. M. Doeff, *Electrochem. Commun.*, 2004, **6**, 767–772.

7 Y. S. Jung, P. Lu, A. S. Cavanagh, C. Ban, G.-H. Kim, S.-H. Lee, S. M. George, S. J. Harris and A. C. Dillon, *Adv. Energy Mater.*, 2013, **3**, 213–219.

8 J. Li, J. M. Zheng and Y. Yang, *J. Electrochem. Soc.*, 2007, **154**, A427.

9 N. Tran, L. Croguennec, C. Jordy, P. Biensan and C. Delmas, *Solid State Ionics*, 2005, **176**, 1539–1547.

10 F. Lin, I. M. Markus, D. Nordlund, T.-C. Weng, H. L. Xin and M. M. Doeff, *Nat. Commun.*, 2014, **5**, 3529, DOI: 10.1038/ncomms4529.

11 S.-K. Jung, H. Gwon, J. Hong, K.-Y. Park, D.-H. Seo, H. Kim, J. Hyun, W. Yang and K. Kang, *Adv. Energy Mater.*, 2013, **4**, 1300787.

12 F. Lin, D. Nordlund, I. M. Markus, T.-C. Weng, H. L. Xin and M. M. Doeff, *Energy Environ. Sci.*, 2014, **7**, 3077–3085.

13 G. V. Zhuang, G. Chen, J. Shim, X. Song, P. N. Ross and T. J. Richardson, *J. Power Sources*, 2004, **134**, 293–297.

14 H.-K. Kim, T.-Y. Seong, W. i. Cho and Y. S. Yoon, *J. Power Sources*, 2002, **109**, 178–183.

15 K. C. Kam and M. M. Doeff, *J. Mater. Chem.*, 2011, **21**, 9991.

16 K. C. Kam, A. Mehta, J. T. Heron and M. M. Doeff, *J. Electrochem. Soc.*, 2012, **159**, A1383–A1392.

17 F. de Groot, M. Grioni, J. Fuggle, J. Ghijsen, G. Sawatzky and H. Petersen, *Phys. Rev. B: Condens. Matter Mater. Phys.*, 1989, **40**, 5715–5723.

18 J. Suntivich, W. T. Hong, Y. Lee, J. M. Rondinelli, W. Yang, J. B. Goodenough, B. Dabrowski, J. W. Freeland and Y. Shao-horn, *J. Phys. Chem. C*, 2014, **118**, 1856–1863.

19 A. R. Armstrong, M. Holzapfel, P. Novák, C. S. Johnson, S.-H. Kang, M. M. Thackeray and P. G. Bruce, *J. Am. Chem. Soc.*, 2006, **128**, 8694–8698.

20 N. Li, R. An, Y. Su, F. Wu, L. Bao, L. Chen, Y. Zheng, H. Shou and S. Chen, *J. Mater. Chem. A*, 2013, **1**, 9760.

21 D. Luo, G. Li, X. Guan, C. Yu, J. Zheng, X. Zhang and L. Li, *J. Mater. Chem. A*, 2013, **1**, 1220.

22 H. Liu, C. R. Fell, K. An, L. Cai and Y. S. Meng, *J. Power Sources*, 2013, **240**, 772–778.

23 S.-H. Kang, W.-S. Yoon, K.-W. Nam, X.-Q. Yang and D. P. Abraham, *J. Mater. Sci.*, 2008, **43**, 4701–4706.

24 W.-S. Yoon, M. Balasubramanian, K. Y. Chung, X.-Q. Yang, J. McBreen, C. P. Grey and D. A. Fischer, *J. Am. Chem. Soc.*, 2005, **127**, 17479–17487.

25 B. Xu, C. R. Fell, M. Chi and Y. S. Meng, *Energy Environ. Sci.*, 2011, **4**, 2223.

26 S. Hwang, W. Chang, S. M. Kim, D. Su, D. H. Kim, J. Y. Lee, K. Y. Chung and E. A. Stach, *Chem. Mater.*, 2014, **26**, 1084–1092.

27 J. Zheng, M. Gu, J. Xiao, P. Zuo, C. Wang and J.-G. Zhang, *Nano Lett.*, 2013, **13**, 3824–3830.

28 F. Yang, Y. Liu, S. K. Martha, Z. Wu, J. C. Andrews, G. E. Ice, P. Pianetta and J. Nanda, *Nano Lett.*, 2014, **14**, 4334–4341.

29 I. M. Markus, F. Lin, K. C. Kam, M. Asta, and M. M. Doeff, 2014 DOI: 10.1021/jz5017526.

30 X. Liu, W. Yang and Z. Liu, *Adv. Mater.*, 2014, DOI: 10.1002/adma.201304676.

31 C. F. Petersburg, Z. Li, N. A. Chernova, M. S. Whittingham and F. M. Alamgir, *J. Mater. Chem.*, 2012, **22**, 19993.

32 X. Liu, D. Wang, G. Liu, V. Srinivasan, Z. Liu, Z. Hussain and W. Yang, *Nat. Commun.*, 2013, **4**, 2568.

33 J. Graetz, C. Ahn, H. Ouyang, P. Rez and B. Fultz, *Phys. Rev. B: Condens. Matter Mater. Phys.*, 2004, **69**, 235103.